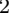


The lens SW05 J143454.4+522850: a fossil group at redshift 0.6?

Philipp Denzel,^{1,2}  Onur Çatmabacak,² Jonathan Coles,³ Claude Cornen,⁴
Robert Feldmann,² Ignacio Ferreras,^{5,6,7} Xanthe Gwyn Palmer,⁸
Rafael Küng,¹ Dominik Leier,⁹ Prasenjit Saha,^{1,2} Aprajita Verma⁸

¹*Physik-Institut, University of Zurich, 8057 Zurich, Switzerland*

²*Institute for Computational Science, University of Zurich, 8057 Zurich, Switzerland*

³*Physik-Department, Technische Universität München, Ernst-Otto-Fischer-Str. 8, 85748 Garching, Germany*

⁴*Zooniverse, c/o Astrophysics Department, University of Oxford, Oxford OX1 3RH, UK*

⁵*Instituto de Astrofísica de Canarias, Calle Vía Láctea s/n, E38205, La Laguna, Tenerife, Spain*

⁶*Department of Physics and Astronomy, University College London, London WC1E 6BT, UK*

⁷*Departamento de Astrofísica, Universidad de La Laguna, E38206 La Laguna, Tenerife, Spain*

⁸*Sub-department of Astrophysics, University of Oxford, Denys Wilkinson Building, Keble Road, Oxford, OX1 3RH, UK*

⁹*Dipartimento di Fisica e Astronomia, Alma Mater Studiorum Università di Bologna, Viale B. Pichat 6/2, 40127, Bologna, Italy*

ABSTRACT

Fossil groups are considered the end product of natural galaxy group evolution in which group members sink towards the centre of the gravitational potential due to dynamical friction, merging into a single, massive, and X-ray bright elliptical. Since gravitational lensing depends on the mass of a foreground object, its mass concentration, and distance to the observer, we can expect lensing effects of such fossil groups to be particularly strong. This paper explores the exceptional system J143454.4+522850. We combine gravitational lensing with stellar population-synthesis to separate the total mass of the lens into stars and dark matter. The enclosed mass profiles are contrasted with state-of-the-art galaxy formation simulations, to conclude that SW05 is likely a fossil group with a high stellar to dark matter mass fraction (0.027 ± 0.003) with respect to expectations from abundance matching (0.012 ± 0.004), indicative of a more efficient conversion of gas into stars in fossil groups.

Key words: Gravitational lensing: strong — galaxies: stellar content — galaxies: formation — dark matter — galaxies: groups: general

1 INTRODUCTION

The currently most tested cosmological concordance model (Λ CDM) provides initial conditions for the formation and evolution of galaxies. Large-scale cosmological simulations serve as a framework which explores different galaxy formation scenarios within Λ CDM from first principles. Although these models differ in their treatment of the baryonic components and the physical mechanisms involved in galaxy formation, the latest generation of simulation suites such as EAGLE (Evolution and Assembly of GaLaxies and their Environments; Crain et al. 2015), FIRE (Feedback In Realistic Environments; Hopkins et al. 2014), and Illustris (Vogelsberger et al. 2014) make remarkably accurate predictions. In particular, they stand in general agreement regarding the growth of primordial density fluctuations by gravitational instability in an expanding Universe, leading to the formation of dark halos.

In direct relation to the interplay between the structure of the dark matter distribution and the baryon physics, galaxies are found in a wide range of structural hierarchies, from low density regions to groups and clusters (see, e.g., Tully 1987; Berlind et al. 2006; Yang et al. 2007), and during their lifetime they experience merging events (e.g. Mamon 1988; Tempel et al. 2017). In some cases, the mergers eventually devoid their entire neighbourhood, leaving behind a single elliptical galaxy of group-scale mass, called a fossil group galaxy (Ponman et al. 1994; Jones et al. 2003). Numerical simulations by Barnes (1989) first motivated such a hierarchical merging scenario (see also Díaz-Giménez et al. 2008). Since then, there have been several supporting reports of X-ray sources identified as fossil groups (Santos et al. 2007; La Barbera et al. 2009). Because most fossil systems found to date lie within $z < 0.2$, fossil galaxy groups most likely are old, undisturbed systems due to the lack of major mergers. While some luminous galaxies experience major merger events in their evolution, fossil group galaxies acquire their mass typically through minor merger events, where the mass ratio stays below 0.3

* Email: phdenzel@physik.uzh.ch

(D’Onghia et al. 2005). Simulations show that a fossil system may assemble half of its mass in dark matter by redshift $z > 1$, and that the assembled mass at any redshift is generally higher in a fossil than in regular groups (Dariush et al. 2007). Since this merging process is relatively fast compared to the cooling time of the surrounding gas, comparable to one to several Hubble times, fossil groups are usually found embedded in giant, X-ray luminous gas halos (Mulchaey 2000). If a fossil system has not yet fully merged, it can be identified by another criterion, a gap in brightness of at least 2 magnitudes (usually defined in the r -band) between the two brightest galaxies in the group (Dariush et al. 2010; Zarattini et al. 2014).

As fossil groups are very massive with a high mass concentration, they can produce strong lensing signatures of background sources (Schirmer et al. 2010). For instance, a massive central group galaxy with mass $M \sim 10^{13} M_{\odot}$ at a cosmological distance of $D \sim 1$ Gpc features an Einstein radius of $(4GM/(c^2 D))^{1/2} \simeq 10''$, which is relatively large compared to typical image separations in single galaxy lenses, which are of order of sub arc-seconds. Strong gravitational lens systems make for exciting, but rare tools for astronomers to independently study galaxies. The morphology of lens systems and their image configurations allow one to infer mass contents and surface density profiles (see, e.g., Treu & Koopmans 2004; Ferreras et al. 2005, 2007; Auger et al. 2010; Leier et al. 2011; Whitaker et al. 2014; Leier et al. 2016; Collett et al. 2017; Nightingale et al. 2019). On that note, it is important to realize that the gravitational deflection of light is independent of the nature of the matter, that is, lensing is equally affected by baryonic and dark matter. While lens models of various forms have been used to constrain mass contents, stellar mass fractions, dark matter profiles, and even cosmological parameters, so far these estimates have not yet been translated to constraints on galaxy formation scenarios. A recent study by Johnson et al. (2018) estimates that a substantial percentage of lensing systems within the group mass range are fossil or pre-fossil groups. If this is indeed the case, models of such lenses could provide a new and independent diagnostic – besides the common criteria to identify fossil groups through X-ray observations – to assess whether a lens in question is in fact a fossil system, in contrast to a more standard group. Thus, models of such lenses could potentially yield constraints on galaxy formation scenarios.

In this paper, we present models for the system J143454.4+522850 (SW05) of the lensing and stellar mass content, followed by a comparison with simulations, which indicate several differences compared with regular early-type galaxies, suggesting the system may indeed be a fossil group.

The paper is organized as follows. In Section 2, the lens system is introduced in detail and its environment thoroughly investigated. Section 3 presents free-form lens models of SW05 and several derived diagnostics in order to obtain a goodness-of-fit estimation. Section 4 describes the methodology yielding light-to-stellar mass estimates from stellar population synthesis models and consequently a spatially 2D-resolved stellar-to-lens mass fraction map. In Section 5 these models are compared to simulated galaxies of similar mass range and Section 6 summarizes the results and discusses the feasibility of SW05 as a fossil group galaxy candidate. Throughout this paper, we adopt a flat cosmology with $(\Omega_m, \Omega_{\Lambda}, H_0^{-1}) = (0.28, 0.72, 13.7 \text{ Gyr})$.

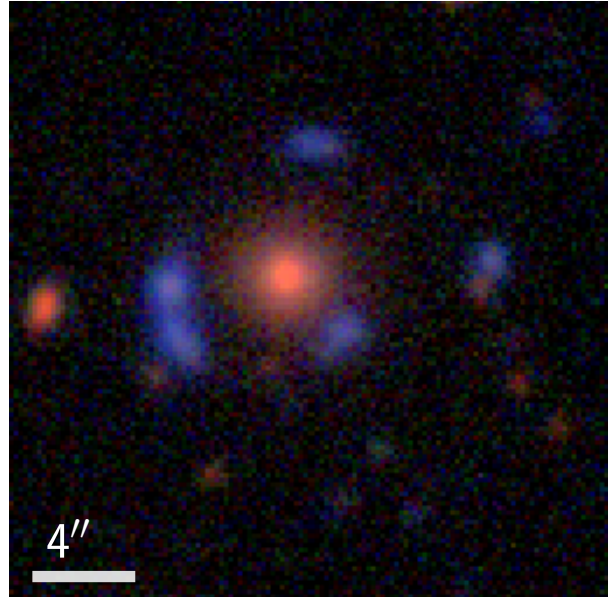


Figure 1. Stacked observational picture of SW05: Observational data from CFHTLS (stored in the CFHT Science Archive) was taken with the wide-field imager MegaPrime in five optical bands (u, g, r, i, and z). The false-colour image was generated using a stacking procedure according to Lupton et al. (2004), where the i, r, and g bands are transformed into rgb colours.

2 THE SYSTEM J143454.4+522850

J143454.4+522850 or SW05 was discovered in the SpaceWarps citizen-science project (More et al. 2016). Out of the 29 promising lens candidates in that work, SW05 probably has the best lens image quality. It is a relatively large gravitational lens with four clearly separated images within a radial distance between 3.5 and 5.25 arcsec from the centre (see Fig. 1). Early models using the image positions suggested a typical four-image galaxy lens (see Appendix A). Subsequently, Küng et al. (2018) identified SW05 as a high-mass galaxy with $\sim 10^{13} M_{\odot}$ and a comparatively high stellar-mass fraction with respect to other galaxies with similar mass. The SW05 lens thus sits at the highest end of the stellar mass distribution of galaxies, making it a very interesting target for follow-up studies.

Originally, the redshift of the lensing galaxy and the background source were determined with the widely used Bayesian photometric redshift estimator **bpz**¹ (Benítez 2000). The code fits the spectral energy distribution (SED) comprising multi-band photometry with a set of well-calibrated templates. The redshift derived by **bpz** for SW05 is $z_L = 0.63 \pm 0.16$. We later cross-matched the sample with Data Release 16 of the Sloan Digital Sky survey (Ahumada et al. 2020) and found a match for the lens in the BOSS survey (Dawson et al. 2012) at $z_L = 0.62525 \pm 0.00020$. The spectrum shows prominent CaII H+K lines along with a substantial 4,000Å break, representative of an old stellar population. In contrast, **bpz** was not able to determine the redshift of the source with enough credibility such that a default redshift from the MegaPipe pipeline was used for the lens model at $z_S = 3.00$. Accurate

¹ <http://www.stsci.edu/~dcoe/BPZ/>

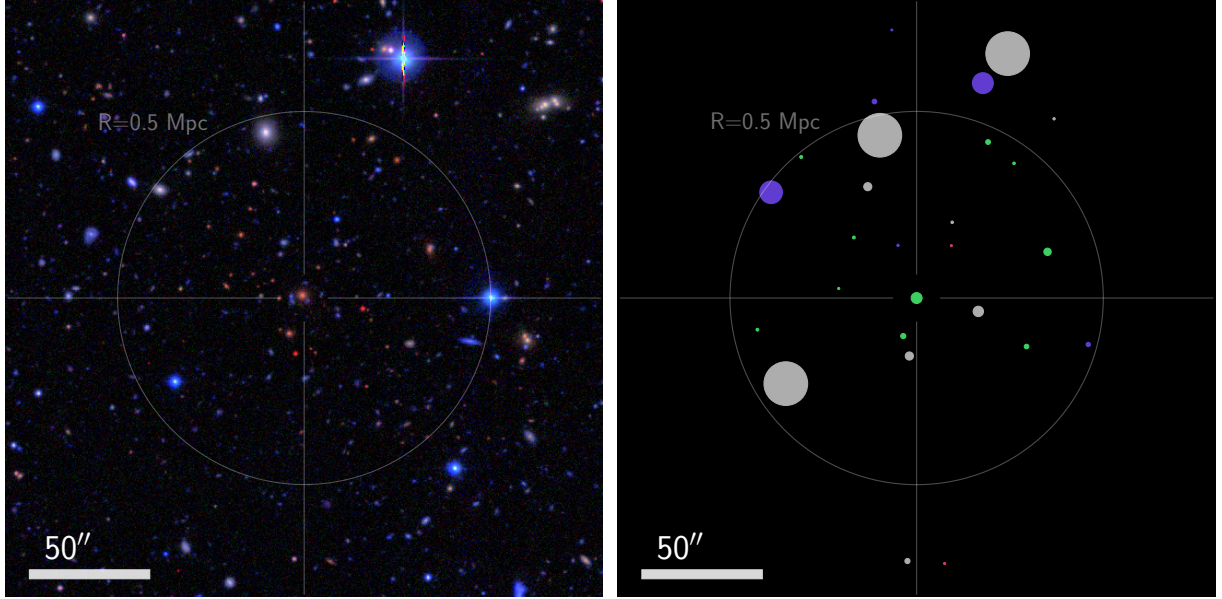


Figure 2. The left panel shows a composite image of the neighbourhood of SW05 from CFHTLS. All the image parameters, including the stacking procedure is the same as for Fig. 1. The panel on the right marks potential group members based on redshift. Green dots represent objects within a redshift range of ± 0.1 of SW05 (including the lens at the centre). Red dots stand for objects further redshifted, blue dots for further blue-shifted objects. Grey dots are stars or unspecified sources. The size of the dots mark the relative brightness. The scale bar has a length of $50''$ which corresponds to a linear distance of roughly 330 kpc at the lens redshift ($z_L=0.625$). For reference, a circumference with radius 0.5 Mpc at the lens plane is shown.

redshifts are not essential for the lensing models, as a change in redshift (of the lens and the source) can be implemented by rescaling the critical surface density, and can therefore easily be adjusted to any other redshift. Moreover, the lens models for SW05 seem to be rather insensitive to changes in the source redshift. Contrarily, a change in lens redshift can considerably impact the results of the photometry-based analysis for the stellar-mass estimation. During the analysis of SW05, spectroscopic redshifts were measured (by XGP and AV) for the source, at around $z_S = 2.6$, and also confirmed the lens redshift. The spectroscopic data was taken with Oxford’s SWIFT spectrograph mounted at the Hale Telescope at the Palomar Observatory.

Fig. 2 shows the wider field of SW05. The left panel shows a $\sim 4 \times 4 \text{ arcmin}^2$ colour image from the CFHTLS data in the g , r , and i filters, with SW05 at the centre. At the lens plane, the image roughly maps the region within 0.8 Mpc of SW05. The right panel shows the sources with a confirmed redshift. The green dots mark galaxies within $\Delta z = \pm 0.1$ of the redshift of SW05, i.e. potential group members (with symbol size scaling with flux). The other dots correspond to sources that cannot be associated to the group of SW05, being either blue- or redshifted with respect to SW05 (coloured accordingly). The grey symbols are stars. A circumference with radius 0.5 Mpc at the lens plane is shown for reference. It is the first indication for SW05 being a fossil group galaxy candidate as its neighbourhood is relatively clear of galaxies at similar brightness and redshift.

3 THE LENSING MASS

The lens modelling was done with the reliable free-form modelling code **GLASS**² (Coles et al. 2014). The free-form technique addresses the many degeneracies present in lens models (Saha 2000; Saha & Williams 2006). In contrast to conventional parametric models, free-form models allow a flexible analysis by constructing the mass distributions $\Sigma(\theta)$ from a high number of base elements. **GLASS** – analogously to the free-form modelling tool **PixeLens** (Saha & Williams 2004) – uses “mass tiles” Σ_n to construct its lens models according to:

$$\Sigma(\theta) = \sum_n \Sigma_n Q(\theta - \theta_n), \quad (1)$$

where Q is a square-pixel profile and θ_n its centroid. The image point positions θ provide the linear constraints on the intrinsic source position β , along with the mass components κ_n . Here, the lens is mapped into 14 rings of pixels around its centre with a total of 497 pixels. However, this does not uniquely define the lens mass distribution and in order to obtain reasonable models, their solution space is further constrained with inequality priors as follows:

- (i) All mass tiles must have non-negative densities: $\Sigma_n \geq 0$.
- (ii) To ensure smoothness in the mass distribution, each mass pixel is limited to twice the average of its neighbours.
- (iii) The local density gradient should point within $\alpha = 45^\circ$ of radially inwards which assures concentration of the lens and more importantly suppresses additional lens images which might appear otherwise.

² <https://ascl.net/1806.009>

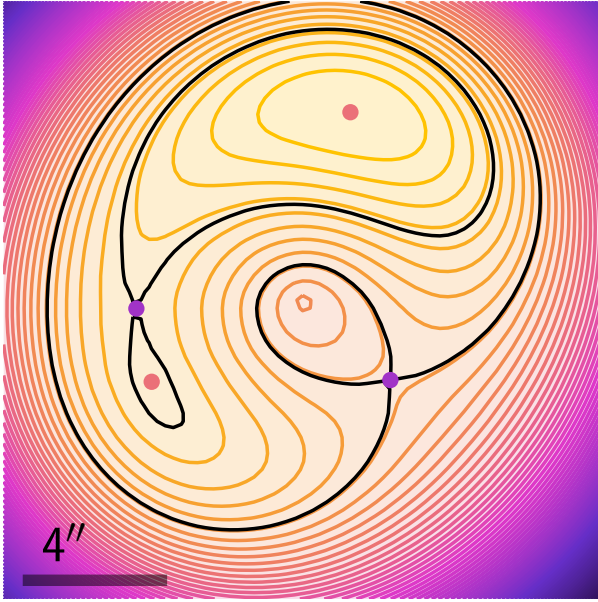


Figure 3. Arrival surface of SW05’s models. This figure shows the light travel times for virtual light paths from the source to the observer. Its maxima, minima, and saddle-points are an illustration of Fermat’s principle, which states that arrival times must be extreme for paths along which light rays travel. The black lines show the saddle-point contours of the surface, the coloured lines general surface contours.

- (iv) The average density $\langle \Sigma \rangle_i$ of mass within a concentric pixel rings is required to not increase with radius. This still allows for twisting iso-density contours and significantly varying ellipticities with radius.

Additionally, to account for any mass component outside the finite model surface, the code allows for a two-component external shear γ . Solutions are then sampled with a customized Monte-Carlo random-walk method (Lubini & Coles 2012). The final model consists of an ensemble of 1000 solution sets of $(\Sigma_n, \beta, \gamma)$ for the image point positions. To verify the validity of the lens models, two main diagnostics are used. Firstly, inspection of the arrival-time surface (see Küng et al. 2015, 2018) is an ideal test to reject certain models in the ensemble, as additional images and uneven contours, indications of unphysical solutions, are easily discernible. Minima, and saddle-points, correspond to points where the gradient of the arrival-time surface is zero and indicate detectable source-image positions. Maxima are usually not detectable as they are highly demagnified. In general the arrival-time surface should:

- (i) reproduce the source image positions on the lens plane,
- (ii) not produce more extrema than the observation shows,
- (iii) have reasonable delay times relative to each other.

Fig. 3 shows the arrival-time surface of the ensemble-average model of SW05.

The high sensitivity of the lens models to the exact image positions is still a troubling issue. An automated search algorithm is quite unreliable due to the generally high signal-to-noise ratios in the data from CFHTLS. Especially with spatially extended images, such as arcs, the correct positions

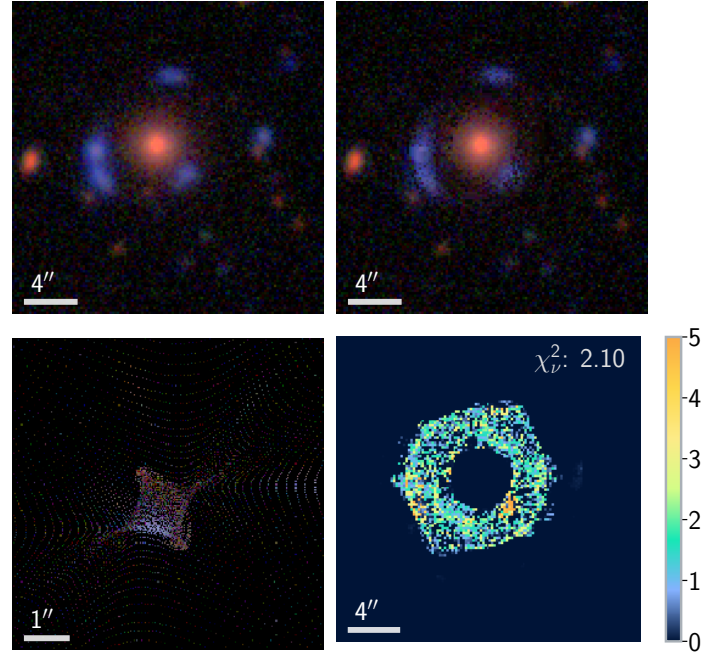


Figure 4. Synthetic-images and source fits from the ensemble-average lens model. Using the modelled lens potential inferred from the mass maps, the observed data (top left) is projected onto the source plane to reconstruct the original source (bottom left). A re-projection onto the image plane results in a synthetic image (top right) which provides a diagnostic, i.e. a visible measure of the models’ accurateness when compared to the observation. The bottom-right panel shows pixel-wise residuals between observed and synthetic data.

are at times arbitrary even in a visual inspection, and a slight shift can cause the mass model of the lens to change moderately, at times even drastically.

Thus, the second diagnostic takes the entire photometric data, rather than single image points, into account by reconstructing the lensed source from the image plane using the mass distribution of the ensemble average solution. This is done with *gleam*³ (Gravitational Lens Extended Analysis Module) (see Denzel et al. 2020 for details). *gleam* uses a simple least-square fitting method to produce synthetic lens images as shown in Fig. 4. Here, the photometric data in the g , r , and i bands were fitted with synthetic images, with an average reduced $\chi^2_\nu \sim 2.10$, and produced synthetic composite images (upper right panel, in contrast with the actual image, shown upper-left). The pixel-wise residuals between observed and synthetic data, scaled by noise, is shown in the bottom-right panel. The reconstructed source composite is shown in the bottom-left panel. These fits provide excellent diagnostics and confirm the validity of the underlying mass model, as the synthetic image is well reproduced in three different bands, and the reconstructed source is relatively consistent. While a match of synthetic images with the observations does not necessarily mean that the true model from the degenerate solution space has been found, the inverse argument can still be used to invalidate a solution.

³ <https://github.com/phdenzel/gleam>

4 THE STELLAR MASS

The surface brightness models of SW05 were obtained by fitting a Sérsic (1968) profile to the CFHT Lens images (Fig. 1) via the Markov-chain Monte-Carlo (MCMC) ensemble sampler `emcee`⁴ (Foreman-Mackey et al. 2013). This feature is part of the `gleam` module. In order to translate the photometric data into a stellar mass map, we obtain the stellar mass-to-light ratio by comparing the colours with population synthesis models, once more adopting the MCMC sampler `emcee`. The base models comprise a set of 12 composite stellar populations from Bruzual & Charlot (2003) that adopt a Chabrier (2003) initial mass function. The 12 models consist of three different choices of metallicity (assumed constant in each case, $[Z/H] = -0.5, 0, +0.3$), and four “time” steps, made by assuming a constant star formation rate over four different time intervals that cover the available time span of SW05. The fitting code explores the parameter space spanned by all linear superpositions of the 12 base models, along with an additional dust attenuation parameter that applies a foreground screen with the Milky Way standard extinction law (Cardelli et al. 1989). For each realization, the observed colours from the full CFHT Lens set u, g, r, i, z are compared with the model predictions to produce a likelihood, from which the best fit and the sampled posterior are used to determine the mass-to-light ratio. We note that while the fits to the actual star formation histories can suffer from degeneracies, the derivation of M/L is more robust.

Finally, the independently derived lensing and stellar mass maps of SW05 were superimposed with a standard 2D interpolation scheme. The result is shown as a stellar-to-lens mass fraction map in Fig. 5, following a similar colour-coded presentation of the values and the uncertainties as in Ferreras et al. (2007). It is a circular 2D false-colour map with 12 mass tiles — or pixels — in radius, which describes the stellar and total surface densities generated from the ensemble. By default, the mass models have a range of almost twice the maximal image separations from the lensing galaxy. Since the image separation of SW05 is relatively large compared to the other lenses discovered in the Space Warps project, its surface density was mapped with a larger pixel scale. For this reason the central region of the lens map was adaptively refined in order to resolve potential cusps. The result is a spatially large map, in which the high concentration of stars in the centre is clearly evident as shown by the redder region. The blue region at larger radii represents lower values of the stellar-to-lens mass fraction, i.e. where dark-matter is the dominant component. The dark matter in the average model mass of SW05 adds up to $(1.12 \pm 0.08) \cdot 10^{13} M_{\odot}$, while the stellar mass amounts to $(3.04 \pm 0.22) \cdot 10^{11} M_{\odot}$. Therefore, the stellar to dark matter fraction in the SW05 lens is 0.027 ± 0.003 . Since the stellar-to-total mass fraction spans a large range, the mass fraction was stretched in the false-colour map with a cube root to make subtle differences in the stellar halo in red colour stretch farther out (assuming that the stellar mass profile is monotonically decreasing) and thus easier to see with the human eye. In general, the galaxy model shows the expected features. If there is any high stellar mass content, it can be found in the centre of the galaxy. The dark matter is located in an extended halo that always dominates

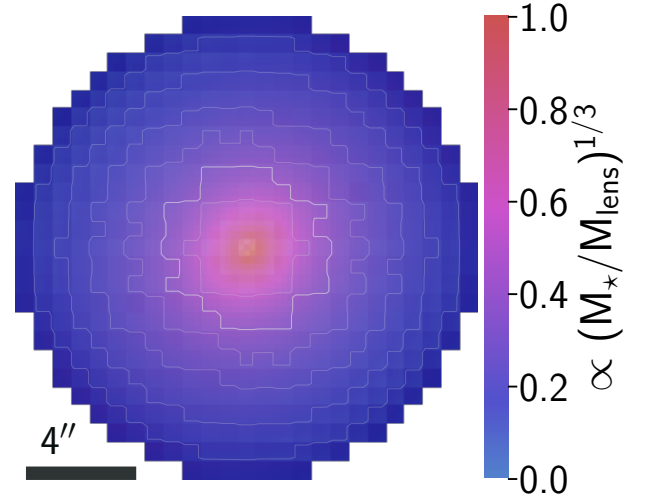


Figure 5. False-colour map of $f = (\Sigma_{\text{stel}}/\Sigma_{\text{lens}})^{e_f}$, i.e. the fraction of stellar to lensing surface mass density in the SW05 lens. Three components were used for the colour mapping, stellar-to-lens surface mass density fraction, namely f , the lensing surface mass density normalization $A = \Sigma_{\text{lens}}^{e_A}$, and the fractional uncertainty $\Delta = (\Sigma_{\text{error}}/\Sigma_{\text{lens}})^{e_{\Delta}}$, where e_f , e_A , and e_{Δ} are arbitrarily adjustable exponents. Those are necessary due to the fact that the visual perception of colours is highly non-linear. With increasing f the colour changes from blue (dominating dark matter content) to red (high stellar mass content). With increasing A the shading changes from dark (low total mass content) to full colour (high total mass content). With increasing Δ , the colour saturation changes from full colour (low uncertainty) to white (high uncertainty). The grey lines describe contours of equal surface density, where the brightest contour indicates the level of critical surface density, i.e. a convergence of 1.

the total matter content, especially towards the outskirts of the galaxy, as previously found in other lensing systems (e.g. Ferreras et al. 2005; Leier et al. 2011).

5 COMPARISON WITH SIMULATIONS

We now contrast the mass profile of the SW05 lens with data corresponding to the formation of massive galaxies in numerical simulations, to determine whether this is a special system compared with the typical mass distribution of this type of galaxies. Fig. 6 shows the cylindrically-averaged cumulative mass profiles. The images lie on the lens plane between 22–38 kpc of the lens centre (vertical dashed lines), and the Einstein radius sits around the middle of this range. The projected mass of the lensing galaxy within the Einstein radius is $\sim (7.01 \pm 1.06) \cdot 10^{12} M_{\odot}$ in dark matter and $\sim (2.58 \pm 0.19) \cdot 10^{11} M_{\odot}$ in stars. At distances of the order of the image separations, the uncertainties in the lens mass are at their lowest. Away from this radial position, the uncertainties grow in both directions, producing a characteristic butterfly-shaped envelope, caused by the well-known steepness degeneracy problem (Saha 2000; Saha & Williams 2006). The shape is only slightly recognizable in this plot, as a logarithmic scaling was used on both axes. A factor alleviating the steepness degeneracy is the comparably high image quality and overall size of the lensing system, which allows for a precise fix of the positions of the images, which in turn makes

⁴ <https://github.com/dfm/emcee>

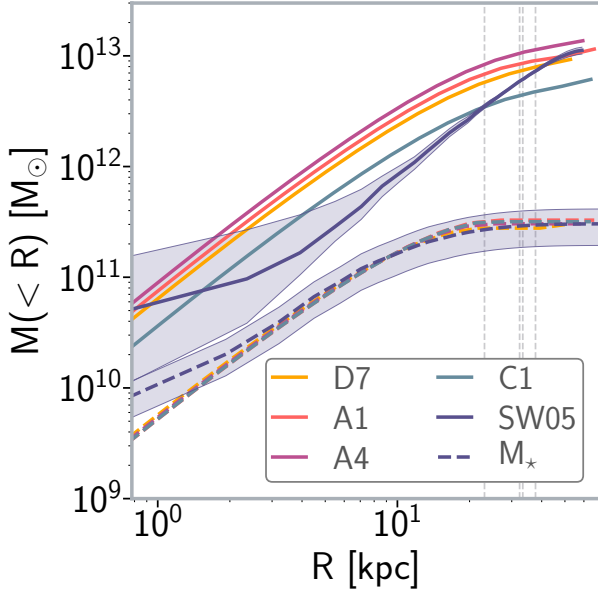


Figure 6. Cumulative mass profiles of the SW05 lensing galaxy models and galaxies from MassiveFIRE simulations (A1, A4, C1, D7 [Feldmann et al. 2016, 2017](#)). The solid curves (lens model in dark-blue) denote the ensemble median of the enclosed total mass. The dashed curves (lens model in dark-blue) give the ensemble median of the enclosed stellar mass. The grey areas show the 99.7% confidence range of the SW05 lens models. The enclosed lens mass is best constrained at the radial location of the images of the background source (vertical thin dotted lines).

the estimation of the total mass content more accurate. The errors in the stellar mass distribution arise from the compatibility of the observed photometric data at the determined redshift with multiple base models to different degrees. The choice of IMF also introduces a systematic uncertainty, but we will see below that our conclusions are not affected by this.

The simulated galaxies shown in Fig. 6 were taken from MassiveFIRE simulations (A1, A4, C1, D7 [Feldmann et al. 2016, 2017](#)). These galaxies were selected due to the comparability of their total mass at redshift $0.5 < z < 0.6$ to SW05. The simulation profiles were recovered with the halo finder AMIGA ([Gill et al. 2004](#); [Knollmann & Knebe 2009](#)). The AMIGA halo finder provides the output as spherically averaged profiles of stellar and dark matter particles. To have a fair comparison however, they were re-averaged within a cylindrical volume, and re-integrated along the z coordinate to yield a projected 2D mass profile of the simulated galaxies. To make the comparison easier, the simulated profiles were scaled in mass to have the same total stellar mass, and in radius to have the same stellar mass at the half-light radius. Among the simulation profiles themselves, there are almost no differences except in the total mass. The enclosed lensing mass profile of SW05 is significantly steeper, and the stellar profile shows differences in the central regions, being shallower than the simulations at $R \sim 1$ kpc. We interpret such differences as a peculiarity of the lens SW05, being a fossil group, thus representing a special environment with respect to other galaxies of similar mass.

6 DISCUSSION

The results presented in this paper suggest that SW05 is one of the most massive lensing galaxies known so far, with an Einstein radius extending to ~ 5 arcsec, that maps into ~ 30 kpc on the lens plane. The stellar to dark matter mass budget can be explored in detail out to the outskirts of the luminous component. Its mass estimate fits the expectations of a massive elliptical galaxy, with a halo mass in the galaxy group range. Its stellar mass dominates the centre, and in total it makes up to 2.7% of the entire mass budget. These results, along with a lack of nearby bright galaxies suggest that SW05 is a fossil group. Fossil groups clear their neighbourhood from any other group members at early times through mergers. If there were any other group members, it would become evident in the lens models as an external shear component giving rise to an ellipticity in the mass maps. In the lens models of SW05 there is little ellipticity to begin with. There seems to be a slight departure from radial symmetry towards the upper left quadrant in Fig. 5. However inspecting Fig. 2, we only find one possible group member candidate, which can be found in the lower left quadrant. The lens models therefore indicate that there is no other major group member in the neighbourhood of SW05, supporting our conclusion. This explanation also seems to fit with the discrepancies found in the comparison with numerical simulations (Fig. 6).

The stellar mass in SW05 accounts for around 2.7% of the total mass. However, this is not necessarily equal to the entire baryonic mass in the lensing galaxy. There could be a substantial mass content in hot, diffuse gas, which would radiate in an energy range of

$$\left(\frac{GM}{c^3}\right) \left(\frac{c}{r}\right) \times 1 \text{ GeV} \sim 5 \times 10^{-8} \text{ keV} \times \left(\frac{M}{M_\odot}\right) \times \left(\frac{r}{\text{pc}}\right)^{-1} \sim 10 \text{ keV.} \quad (2)$$

This falls in the X-ray spectral window, of which no observational data was taken so far. Another indication of the special nature of the SW05 lens can be obtained through a dynamical tracer such as velocity dispersion. The available SDSS/BOSS spectrum gives a value for the stellar component, within the 2 arcsec diameter fiber of the spectrograph of $\sigma = 256 \pm 32$ km/s. Moreover, we can use the proxy from lensing data proposed by [Leier \(2009\)](#), namely:

$$\sigma^2 = \frac{2}{3\pi} \frac{GM(<r)}{r}, \quad (3)$$

shown in Fig. 7. The figure also shows the values of σ for the simulations, that reach a maximum at smaller galactocentric radii compared to SW05. This also means that the total mass of SW05 could be well above $10^{13} M_\odot$ if the galaxy model were to be extended to larger radii.

The velocity dispersion can formally be converted into a temperature with

$$T(r) = \frac{m_p \sigma(r)^2}{e} \quad (\text{eV}) \quad (4)$$

where m_p is the proton mass, $\sigma(r)$ the velocity dispersion profile, and e the elementary charge. The right y -axis of Fig. 7 shows such a conversion. This temperature should be of the same order as the temperature at which the gas in the outskirts of the galaxy radiates. The maxima for the observed and simulated galaxies have values around $\sigma \sim 400$ km/s and $T \sim 2$ keV.

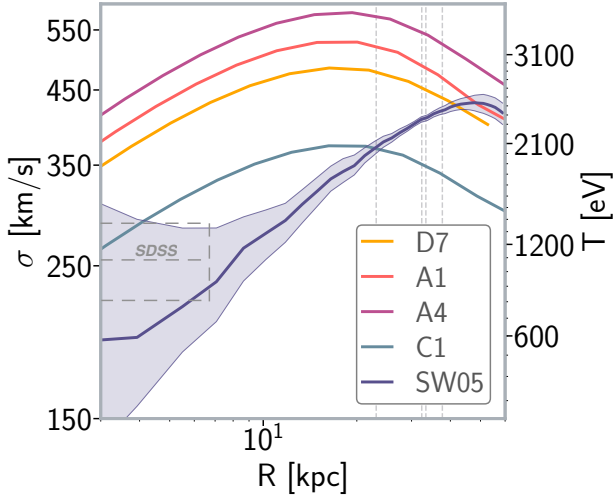


Figure 7. Velocity dispersion profile of SW05, contrasted with galaxies from simulations: σ is formally derived from the mass profiles shown in Fig. 6 according to Eq. (3). On the right y-axis the corresponding temperature values are denoted in units of eV according to Eq. (4). The grey dashed lines mark the observed estimate from the SDSS/BOSS spectrum ($\sigma=256\pm32$ km/s) and extends horizontally to map the fibre of the spectrograph.

We also contrast the total stellar to dark matter mass ratio found in SW05 with the standard abundance matching (AM) trends. These trends are obtained by comparing the halo mass function of numerical simulations with the stellar mass function from observational data. Such a comparison allows us to determine the variation in the stellar to dark matter mass fraction as a function of halo mass, a signature of overall star formation efficiency. Fig. 8 compares our estimate of this fraction for the SW05 lens (1σ error bars) with the AM relation of Moster et al. (2010), shown as a line and a shaded region that encompasses the 1σ uncertainties of the trend at the lens redshift ($z_L=0.625$). The AM relation features a well-known peak at a halo mass around $M_h \sim 10^{12} M_\odot$ with a stellar-to-dark matter mass fraction $\sim 2\%$, followed by a decreasing trend with increasing halo mass. At the mass of SW05, the AM relation gives a stellar to dark matter fraction of 0.012 ± 0.004 , well below the observed value for SW05 (0.027 ± 0.003), suggesting that the conversion of gas into stars in this galaxy has been significantly higher than the average, at similar mass, and even higher than the peak of the relation at the same redshift. Such a result could be expected within our fossil group hypothesis, if we consider that in such a special environment – where merging and/or infall processes lead to the formation of the central massive galaxy – took place at very early cosmic time, when there was larger gas reservoirs to fuel star formation. This may represent a clear signature to identify fossil groups.

In conclusion, the study presented in this paper identifies a rare gravitational lens of group mass-scale as a fossil group candidate at intermediate redshift, with a significantly high stellar-to dark matter mass fraction with respect to the expectations from abundance matching. In the future, this analysis could very well be applied to other lensing groups to help in the identification of fossil groups.

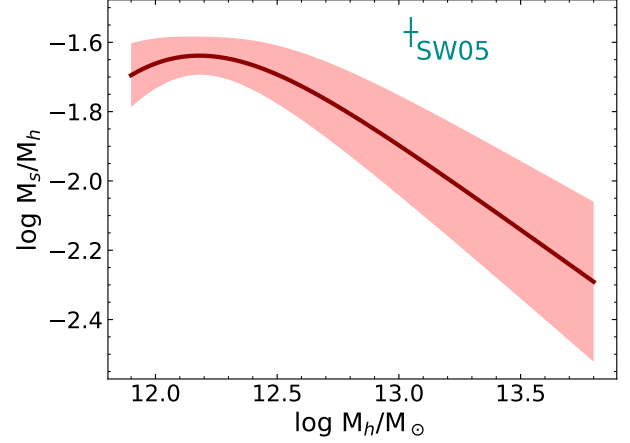


Figure 8. The stellar to dark matter mass fraction is shown as a function of the halo mass. The solid line and (1σ) shaded region represent the standard abundance matching relation, at the redshift of the lens $z_L=0.625$, taken from Moster et al. (2010). The error bars for the SW05 lens are given at the 1σ confidence level.

ACKNOWLEDGMENTS

PhD acknowledges support from the Swiss National Science Foundation.

This work is based on observations obtained with MegaPrime/MegaCam, a joint project of CFHT and CEA/IRFU, at the Canada-France-Hawaii Telescope (CFHT) which is operated by the National Research Council (NRC) of Canada, the Institut National des Sciences de l'Univers of the Centre National de la Recherche Scientifique (CNRS) of France, and the University of Hawaii. This research used the facilities of the Canadian Astronomy Data Centre operated by the National Research Council of Canada with the support of the Canadian Space Agency. CFHTLenS data processing was made possible thanks to significant computing support from the NSERC Research Tools and Instruments grant program.

DATA AVAILABILITY

The data underlying this article are available at the Canadian Astronomy Data Centre (<https://www.cadc-ccda.hia-ihia.nrc-cnrc.gc.ca/>; details are cited in the acknowledgements). The derived data generated in this research will be shared on request to the corresponding author.

REFERENCES

- Ahumada R., et al., 2020, *ApJS*, 249, 3
- Auger M. W., Treu T., Bolton A. S., Gavazzi R., Koopmans L. V. E., Marshall P. J., Moustakas L. A., Burles S., 2010, *ApJ*, 724, 511
- Barnes J. E., 1989, *Nature*, 338, 123
- Benítez N., 2000, *ApJ*, 536, 571
- Berlind A. A., et al., 2006, *ApJS*, 167, 1
- Bruzual G., Charlot S., 2003, *MNRAS*, 344, 1000
- Cardelli J. A., Clayton G. C., Mathis J. S., 1989, *ApJ*, 345, 245
- Chabrier G., 2003, *PASP*, 115, 763
- Coles J. P., Read J. I., Saha P., 2014, *MNRAS*, 445, 2181

Collett T. E., et al., 2017, *ApJ*, 843, 148
 Crain R. A., et al., 2015, *MNRAS*, 450, 1937
 D’Onghia E., Sommer-Larsen J., Romeo A. D., Burkert A., Pedersen K., Portinari L., Rasmussen J., 2005, *ApJ*, 630, L109
 Dariush A., Khosroshahi H. G., Ponman T. J., Pearce F., Raychaudhury S., Hartley W., 2007, *MNRAS*, 382, 433
 Dariush A. A., Raychaudhury S., Ponman T. J., Khosroshahi H. G., Benson A. J., Bower R. G., Pearce F., 2010, *MNRAS*, 405, 1873
 Dawson K. S., et al., 2012, *AJ*, 145, 10
 Denzel P., Mukherjee S., Coles J. P., Saha P., 2020, *MNRAS*, 492, 3885–3903
 Díaz-Giménez E., Muriel H., Mendes de Oliveira C., 2008, *A&A*, 490, 965
 Feldmann R., Hopkins P. F., Quataert E., Faucher-Giguère C.-A., Kereš D., 2016, *MNRAS: Letters*, 458, L14
 Feldmann R., Quataert E., Hopkins P. F., Faucher-Giguère C.-A., Kereš D., 2017, *MNRAS*, 470, 1050
 Ferreras I., Saha P., Williams L. L. R., 2005, *ApJ*, 623, L5
 Ferreras I., Saha P., Burles S., 2007, *MNRAS*, 383, 857
 Foreman-Mackey D., Hogg D. W., Lang D., Goodman J., 2013, *PASP*, 125, 306
 Gill S. P. D., Knebe A., Gibson B. K., 2004, *MNRAS*, 351, 399
 Hopkins P. F., Kereš D., Oñorbe J., Faucher-Giguère C.-A., Quataert E., Murray N., Bullock J. S., 2014, *MNRAS*, 445, 581
 Johnson L. E., Irwin J. A., White III R. E., Wong K.-W., Maksym W. P., Dupke R. A., Miller E. D., Carrasco E. R., 2018, *ApJ*, 856, 131
 Jones L. R., Ponman T. J., Horton A., Babul A., Ebeling H., Burke D. J., 2003, *MNRAS*, 343, 627
 Knollmann S. R., Knebe A., 2009, *ApJS*, 182, 608
 Küng R., et al., 2015, *MNRAS*, 447, 2170
 Küng R., et al., 2018, *MNRAS*, 474, 3700
 La Barbera F., R. de Carvalho R., G. de la Rosa I., Sorrentino G., Gal R. R., Kohl-Moreira J. L., 2009, *AJ*, 137, 3942
 Leier D., 2009, *MNRAS*, 400, 875
 Leier D., Ferreras I., Saha P., Falco E. E., 2011, *ApJ*, 740, 97
 Leier D., Ferreras I., Saha P., Charlot S., Bruzual G., La Barbera F., 2016, *MNRAS*, 459, 3677
 Lubini M., Coles J., 2012, *MNRAS*, 425, 3077
 Lupton R., Blanton M. R., Fekete G., Hogg D. W., O’Mullane W., Szalay A., Wherry N., 2004, *PASP*, 116, 133
 Mamon G. A., 1988, in Audouze J., Pelletan M.-C., Szalay A., Zel’dovich Y. B., Peebles P. J. E., eds, IAU Symposium Vol. 130, Large Scale Structures of the Universe. p. 545
 More A., et al., 2016, *MNRAS*, 455, 1191
 Moster B. P., Somerville R. S., Maubetsch C., van den Bosch F. C., Macciò A. V., Naab T., Oser L., 2010, *ApJ*, 710, 903
 Mulchaey J. S., 2000, *ARA&A*, 38, 289
 Nightingale J. W., Massey R. J., Harvey D. R., Cooper A. P., Etherington A., Tam S.-I., Hayes R. G., 2019, *MNRAS*
 Ponman T. J., Allan D. J., Jones L. R., Merrifield M., McHardy I. M., Lehto H. J., Luppino G. A., 1994, *Nature*, 369, 462
 Saha P., 2000, *AJ*, 120, 1654
 Saha P., Williams L. L. R., 2004, *AJ*, 127, 2604
 Saha P., Williams L. L. R., 2006, *ApJ*, 653, 936
 Santos W. A., Mendes de Oliveira C., Sodr  Jr. L., 2007, *AJ*, 134, 1551
 Schirmer M., Suyu S., Schrabback T., Hildebrandt H., Erben T., Halkola A., 2010, *A&A*, 514, A60
 S rsic J. L., 1968, Atlas de Galaxias Australes. Observatorio Astronómico, Universidad Nacional de Córdoba
 Tempel E., Tuvikene T., Kipper R., Libeskind N. I., 2017, *A&A*, 602, A100
 Treu T., Koopmans L. V. E., 2004, *ApJ*, 611, 739
 Tully R. B., 1987, *ApJ*, 321, 280
 Vogelsberger M., et al., 2014, *MNRAS*, 444, 1518

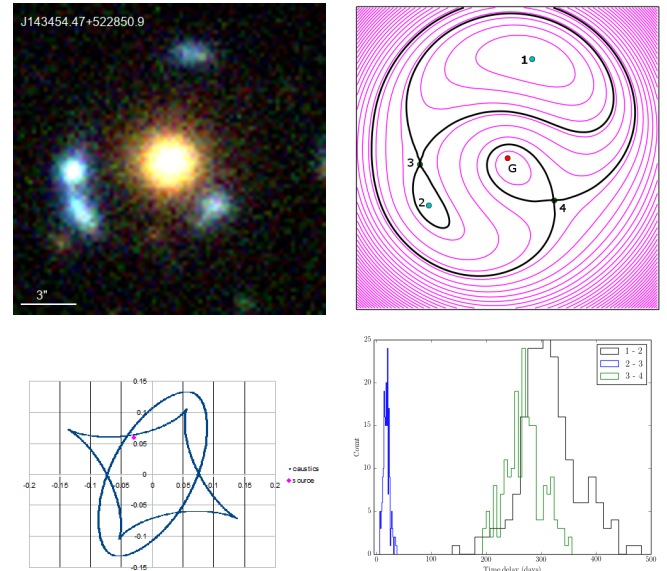


Figure A1. Early results from Space Warps indicating that SW05 is indeed a lensing system. Upper left: a false-colour image enhancing the candidate lensed images. Lower left: Possible caustic configuration. Upper right: Arrival time surface, similar to Fig. 3 indicating the inferred image order. Lower right: Histograms of model time delays between the images.

Whitaker K. E., Rigby J. R., Brammer G. B., Gladders M. D., Sharon K., Teng S. H., Wuyts E., 2014, *ApJ*, 790, 143
 Yang X., Mo H. J., van den Bosch F. C., Pasquali A., Li C., Barden M., 2007, *ApJ*, 671, 153
 Zarattini S., et al., 2014, *A&A*, 565, A116

APPENDIX A: EARLY MODELS

As mentioned in Section 2 the SW05 was discovered in the Space Warps citizen-science project, appearing as one of 29 promising lens candidates in More et al. (2016). As an especially interesting candidate, SW05 had been discussed in the Space Warps online forum since 2013, under the name ASW0007k4r, which was the Space Warps internal name for the particular field containing the object. Fig. A1 shows some early results discussed on the forum. As well as a false-colour image that highlights the possible lensed images, there are models for caustics indicating a near-fold system, an arrival-time surface, and histograms of model time delays between consecutive images, in the event that the source galaxy has a variable source.